

Finite-range time delays in numerical attosecond-streaking experiments

Jing Su, Hongcheng Ni, Andreas Becker, and Agnieszka Jaroń-Becker

JILA and Department of Physics, University of Colorado, Boulder, Colorado 80309-0440, USA

(Received 19 February 2013; published 12 August 2013)

We present results of numerical simulations and theoretical classical analysis of time delays with respect to the instant of ionization in a numerical streaking experiment. We show that the time delay is related to a finite range in space, which the emitted electron probes after its transition into the continuum until the streaking pulse ceases. This finite-range time delay results from the coupling of the atomic potential and the streaking field and strongly depends on the parameters, in particular the duration, of the streaking field. It can be represented as an integral or sum over piecewise field-free time delays weighted by the ratio of the instantaneous streaking field strength relative to the field strength at the instant of ionization.

DOI: [10.1103/PhysRevA.88.023413](https://doi.org/10.1103/PhysRevA.88.023413)

PACS number(s): 33.80.Rv, 33.80.Wz

I. INTRODUCTION

Advances in extreme ultraviolet (XUV) laser radiation technology have enabled the generation of single pulses as short as about 100 as (1 as = 10^{-18} s). This makes it possible to study the temporal dynamics of quantum processes, such as a photoionization, on an unprecedented time scale [1]. Recently, experiments [2–4] have been performed to observe whether the photoemission of an electron follows instantly the variation of the incident light field. Among them, some measurements used the attosecond streaking technique [5], in which the momentum of the electron, emitted due to the interaction with an ultrashort XUV laser pulse, gets varied by a superimposed weak streaking field. The momentum (or energy) of the photoelectron is then observed as a function of the delay between the XUV and streaking pulses. Comparison of the oscillating streaking patterns for electron emission from different atomic shells [3] (or bands in the solid [2]) revealed temporal offsets, which were attributed as a relative delay in the photoemissions.

Originally, in the attosecond streaking technique the electron dynamics in the continuum was approximated as that of a free particle in the streaking field with momentum $\mathbf{k}_f^{(0)}(t_i) \simeq \mathbf{k}_0 - \mathbf{A}_s(t_i)$, where $k_0 = \sqrt{2(\omega - I_p)}$ is the streaking-field-free asymptotic momentum and $\mathbf{A}_s(t_i)$ is the vector potential of the streaking field at the time of ionization t_i [6]. The effect of the simultaneous interaction of the electron with the ionic potential and the streaking field is neglected in this approximation. Hence, theoretical analysis focuses on the following aspects: How is the observed offset related to the Wigner-Smith (WS) time delay [7,8] that measures the delay of an electron propagating in a potential towards infinity as compared to a freely propagating electron [3,9–18]? Which effect does the streaking laser pulse, in particular the coupling between this field and the atomic potential, have on the observed time delays [13–22]? Do short- and long-range parts of these interactions have to be separated [13–17]?

In previous theoretical analysis the temporal offset is often separated into a sum of the field-free WS time delay and a contribution induced by the coupling of the Coulomb potential and the streaking field [13–21]. This separation promptly provokes the concern that the WS time delay diverges for a long-range potential such as the Coulomb interaction between an electron and its residual ion [8,23,24]. In the theoretical

analysis the corresponding term is therefore often limited to a short-range part of the Coulomb interaction.

Results of our numerical simulations and theoretical analysis show that the temporal offset in numerical simulations is determined by the electron dynamics in the combined potential of the Coulomb and the streaking fields over a *finite range* in time and space until the streaking pulse ceases. Due to the strong impact of the parameters of the streaking field, the streaking time delay can be represented as a sum of piecewise field-free time delays weighted by the instantaneous streaking field strength normalized to the field strength at the instant of ionization [25]. The important aspect of this finite-range interaction (a) removes any concerns about the divergence of the WS delay from theoretical discussions, (b) makes an *a priori* separation of short- and long-range parts of the interaction unnecessary, and (c) links the observation of a time delay to the detection of electrostatic potentials over larger distances.

The paper is organized as follows. We first use the results of numerical one-dimensional (1D) model calculations to demonstrate the dependence of the streaking time delay on the finite propagation distance of the electron wave packet until the streaking pulse ceases. Next, we present a classical analysis of the electron dynamics that further supports our conclusions. Theoretical limits and the relation to the WS time delay as well as subtle features in the numerical results are then discussed based on the classical analysis. We conclude by presenting applications to three-dimensional (3D) cases and end with a summary of our results.

II. FINITE-RANGE TIME DELAY

A. Quantum simulations

We first consider the photoemission of an electron by an ultrashort XUV laser field, which is initially bound in

$$V(x) = V_{CG}(x) = -\frac{Z}{\sqrt{x^2 + a}} + V_0 e^{-\left(\frac{|x-x_0|}{\sigma}\right)^2}. \quad (1)$$

$V_{CG}(x)$ consists of a Coulomb potential centered at $x = 0$ with effective charge Z and soft-core parameter a and a second potential of Gaussian shape with depth V_0 and width σ centered at a distance x_0 from the center of the Coulomb potential. We investigate the influence of the Gaussian potential on the

streaked momentum of the photoelectron. In order to clearly show the effects, we have chosen potential parameters as $Z = 3.0$, $a = 2.0$, $\sigma = 2.0$, and $V_0 = -0.5, -2.0$, and -4.0 . However, our conclusions do not depend on the choice of these parameters. In all simulations the initial state is chosen to be the ground state of the Coulomb potential, which has an energy of -1.7118 and is not affected by the Gaussian potential as long as $x_0 \geq 20$.

We simulate a streaking experiment by numerically solving the time-dependent Schrödinger equation (TDSE) representing the interaction of the electron with $V(x)$, an XUV field E_{XUV} , and a streaking field E_s ,

$$i \frac{\partial \Psi(x,t)}{\partial t} = \left\{ \frac{p^2}{2} + V(x) + [E_{\text{XUV}}(t) + E_s(t)]x \right\} \Psi(x,t), \quad (2)$$

where p is the momentum operator and $E(t) = E_0 \sin^2(\pi t/T) \cos(\omega t + \phi)$ for both laser fields with peak amplitude E_0 , pulse duration T , central frequency ω , and carrier-envelope phase (CEP) ϕ of the respective field. We solve Eq. (2) on a grid of size of 14 000 (from -7000 to 7000) with $\Delta x = 0.05$ and $\Delta t = 0.01$ using the Crank-Nicolson method. We propagated the wave function over long times and large distances well after XUV and streaking fields have ceased and the outgoing wave packet has passed the Gaussian potential. The grid was chosen large enough such that the wave function did not reach the boundaries. We obtained the electron momentum spectrum by spatially separating the outgoing part of the wave function from the remaining (bound) part close to the center of the grid and then performing a Fourier transform. We have checked that any error due to the finite grid size or the plane-wave projection is negligibly small. By varying the delay t_i between the XUV and the streaking pulses over the central cycle of the streaking field, we obtained the streaked momentum of the photoelectron k_f as a function of t_i . As pointed out before (e.g., [5,12–14]), the distribution has a temporal offset or delay Δt_s with respect to the vector potential at t_i , which can be extracted by fitting $k_f(t_i)$ to $k_0 - \alpha A_s(t_i + \Delta t_s)$, with a fitting parameter $\alpha \simeq 1$.

We consider photoemission from the initial state by an XUV pulse with $I_{\text{XUV}} = 1 \times 10^{15}$ W/cm², $\omega_{\text{XUV}} = 100$ eV, $T_{\text{XUV}} = 600$ as, and $\phi_{\text{XUV}} = -\pi/2$. The parameters of the streaking pulse were $I_s = 1 \times 10^{12}$ W/cm², $\lambda_s = 800$ nm, and $\phi_s = -\pi/2$. In Fig. 1(a), we show the extracted values for the delay Δt_s (stars, squares, and circles) for different positions x_0 of the Gaussian potential and a streaking pulse having eight cycles. The delay Δt_s strongly varies when the Gaussian potential is located close to the center of the Coulomb potential and the amplitude of this variation increases with an increase of the depth of the Gaussian potential. However, independent of the strength of the Gaussian potential, Δt_s remains constant for $x_0 > x_{\text{finite}} \simeq 850$, for which we obtained the same numerical result with and without (diamond) the Gaussian potential. Our simulations show that at the end of the streaking pulse the center of the outgoing electron wave packet was located at $x_{\text{finite}} \simeq 850$. Thus, Δt_s accounts for the presence of the Gaussian potential only when the electron wave packet reaches the potential before the interaction with the streaking pulse ceases.

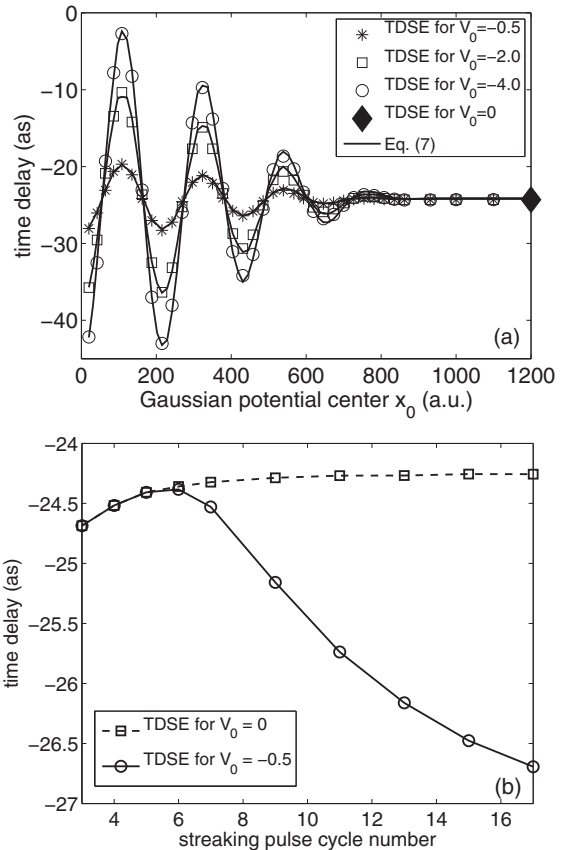


FIG. 1. (a) Δt_s as a function of the position x_0 of the Gaussian potential. We compare results of TDSE (stars, squares, and circles for $V_0 = -0.5, -2.0$, and -4.0 , respectively) with those of classical calculations, Eq. (7) (lines). Also shown is the TDSE result without Gaussian potential (diamond on the right end). In the classical calculations the parameter α varied between 0.985 and 1.084. (b) Comparison of Δt_s from TDSE for different cycle numbers of the streaking pulse with (solid line with circles) and without (dashed line with squares) the Gaussian potential. The Gaussian potential was located at $x_0 = 650$. Other parameters are given in the text.

To confirm this conclusion, we determined Δt_s for streaking pulses having different durations while the Gaussian potential remains located at $x_0 = 650$. For short streaking pulses ($N_s \leq 5$) we again obtained the same results for Δt_s in simulations with [Fig. 1(b), solid line with circles] and without (dashed line with squares) the Gaussian potential. In each of these simulations the outgoing wave packet was located at $x < x_0 = 650$ at the end of the streaking pulse. In contrast, as soon as the outgoing wave packet reaches x_0 for $N > 5$, Δt_s deviates from the result obtained in simulations without the Gaussian potential.

B. Classical analysis

It is known that in strong-field physics the propagation of an electron in the continuum can be often well described by classical analysis (e.g., [26]). We therefore make use of this method to gain further insights into our results. After the transition into the continuum due to XUV photon absorption the dynamics of the electron in the general 3D case is

given by

$$\frac{d\mathbf{k}}{dt} = -\mathbf{E}_s(t) - \nabla V(\mathbf{r}). \quad (3)$$

For a linearly polarized field the simultaneous interaction of the electron with the field and the potential takes effect along the direction of the polarization, which we choose as the x axis:

$$\frac{dk}{dt} = -E_s(t) - \frac{dV}{dx}. \quad (4)$$

By multiplying dx to both sides of Eq. (4) and then integrating it, the solution of Eq. (4) for the asymptotic momentum of the electron at $x \rightarrow \infty$ can be written as [27]

$$\begin{aligned} k_f(t_i) &= \sqrt{k_i^2 + 2V(x_i) - 2 \int_{t_i}^T E_s(t)k(t)dt} \\ &= \sqrt{k_0^2 - 2 \int_{t_i}^T E_s(t)k(t)dt}, \end{aligned} \quad (5)$$

with $k_0 = \sqrt{k_i^2 + 2V(x_i)} = \sqrt{2(\omega - I_p)}$, t_i the time, and x_i the location of photoelectron emission. By setting this result equal to [for $E_s(t_i) \neq 0$]

$$k_f(t_i) = k_0 - \alpha A_s(t_i + \Delta t_s) \simeq k_0 - \alpha A_s(t_i) + \alpha E_s(t_i)\Delta t_s, \quad (6)$$

as used in the fitting of the streaking results, we get

$$\Delta t_s \simeq \frac{\alpha A_s(t_i) + \sqrt{k_0^2 - 2 \int_{t_i}^T E_s(t)k(t)dt} - k_0}{\alpha E_s(t_i)}. \quad (7)$$

It has been previously shown (e.g., [13,14]) that the results of classical streaking simulations depend on the choice of the initial position x_i . We have chosen x_i to be the most probable position of the electron in the initial state [e.g., $x_i = 0$ for $V_{CG}(x)$]. Alternatively, one can sample the initial conditions in Monte Carlo calculations (see, e.g., [13]). To make use of the classical analysis we further note that the temporal offset Δt_s in Eq. (7) depends on the choice of α . We determined α such that Δt_s remains approximately constant while varying t_i over one field cycle (solid line with squares in Fig. 2). Please note that, independent of the choice of α , our classical prediction for Δt_s diverges for $E_s = 0$.

As exemplified in Fig. 1(a), our classical predictions for Δt_s (solid lines) agree very well with the TDSE results (points). In the comparison we have chosen liberation of the electron at the peak of the streaking field within its central cycle. Our results so far have a few important implications: Δt_s depends on the coupling between the streaking field and the (atomic) potential and, thus, on the parameters of the streaking field $E_s(t)$ itself. Consequently, the time delay is determined by the electron dynamics in the combined potential of the Coulomb and streaking fields over a *finite range* in time and space until the streaking pulse ceases at $t = T$. In view of this result any previously raised theoretical concerns about a diverging WS time delay are unnecessary. Our findings further imply that a separation of short- and long-range parts of the interactions for the analysis is not necessary. Finally, our results indicate that the presence of an additional potential at a distance of

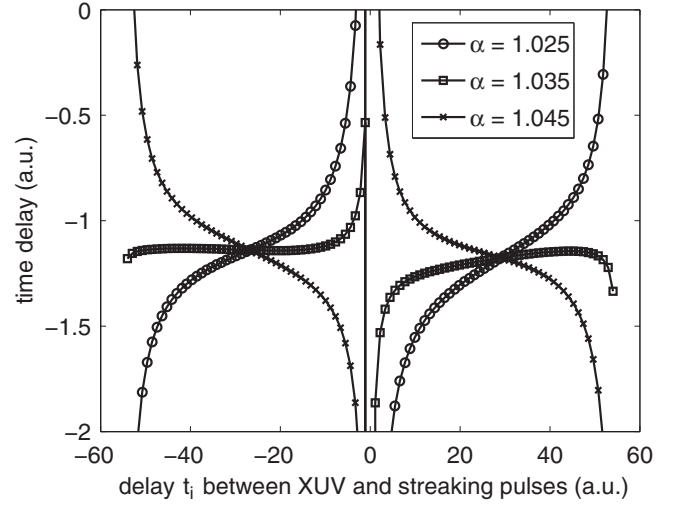


FIG. 2. Classical predictions for the time delay as a function of the delay between XUV ionizing and IR streaking pulses for different fitting parameter α by using Eq. (7). Calculations are performed for the 1D potential $V_{CG}(x)$ in Eq. (1) with $Z = 3.0$, $a = 2.0$, $V_0 = -0.5$, $\sigma = 2.0$, and $x_0 = 20$.

the original location of the photoelectron can be detected by observing Δt_s over different cycles of the streaking pulse.

C. Wigner-Smith time delay and theoretical limits

To study the relation of the finite-range time delay Δt_s to the field-free WS time delay we further simplify Eq. (7). By noting that the momentum shift $k_f(t_i) - k_0$ in Eq. (5) is usually small, we can expand the square root to first order. Assuming $\alpha = 1$, we obtain

$$\Delta t_s \simeq \frac{1}{E_s(t_i)} \int_{t_i}^T E_s(t) \left(1 - \frac{k(t)}{k_0}\right) dt, \quad (8)$$

which provides accurate results for liberation of the electron at the peak of $E_s(t)$ within its central cycle. It is now instructive to further rewrite Eq. (8) as a sum by assuming that the streaking field and the electron momentum are approximately constant in the time interval $[t_j, t_j + \delta t]$, i.e., $E_s(t) \simeq E_s(t_j)$ and $k(t) \simeq k(t_j)$,

$$\Delta t_s \simeq \frac{1}{E_s(t_i)} \sum_{j=1}^N E_s(t_j) \left(1 - \frac{k(t_j)}{k_0}\right) \delta t \quad (9)$$

$$\simeq \sum_{j=1}^N \frac{E_s(t_j)}{E_s(t_i)} \Delta t_{\text{field-free}}^{(j)}. \quad (10)$$

In Eq. (10) we further assumed that the streaking field $E_s(t_j)$ is weak as compared to $V(x)$ and thus $k(t_j)$ approximately depends only on $V(x)$ [23]. $\Delta t_{\text{field-free}}^{(j)}$ is a finite-range piecewise field-free time delay that the electron accumulates during its propagation in the time interval $[t_j, t_j + \delta t]$ and over a related finite region $[x_j, x_j + \delta x]$ of the potential $V(x)$ as compared to the propagation of a free particle over the same distance in space.

Equation (10) provides us with an interesting interpretation of the observed time delay: It is neither the WS time delay Δt_{WS} nor the simple sum of finite-range piecewise field-free

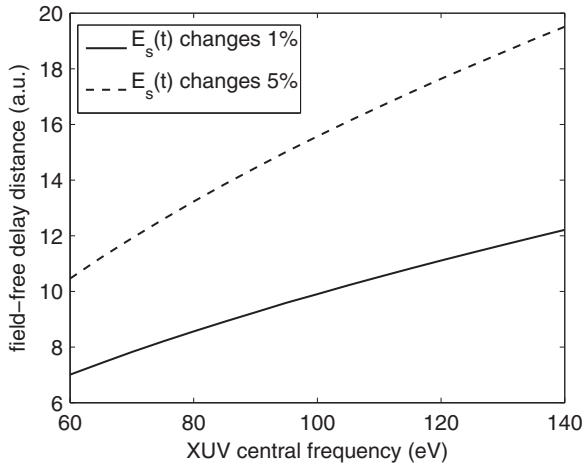


FIG. 3. Classical estimates for the “field-free” delay distance of an electron, released at the peak of a three-cycle streaking pulse (wavelength of 800 nm) in the 1D Coulomb potential [i.e., $V_0 = 0$ in Eq. (1)], as a function of the XUV photon energy. This distance was determined by the position of the electron at the time instant when the streaking field changed to 99% (solid line) and 95% (dashed line) of the peak field strength.

time delays. Instead, the piecewise field-free time delays are weighted by the streaking field strength present when the electron wave packet propagates over the corresponding part of the potential. Thus, we can conclude that the streaking time delay strongly depends on the electron dynamics in the coupled atomic and time-varying streaking field potential.

In earlier work (e.g. [14,15,17]) the streaking time delay was often separated into the sum of the field-free WS time delay and a contribution accounting for the coupling. Although we do not derive such a relation, we note that in Eq. (10) $E_s(t_1) \simeq E_s(t_i)$ and therefore the first term of the sum is equal to the field-free time delay, which the electron acquires during $[t_i, t_i + \delta t]$. The corresponding “field-free” delay distance over which the electron travels during this time interval depends on the electron energy (or XUV frequency) and the wavelength of the streaking field. In Fig. 3 we present classical estimates for this distance assuming that the electron is emitted at the peak of a three-cycle near-infrared laser pulse. We note that the calculated “field-free” delay distances are approximately equal to short-range distances of atomic potentials.

Equation (10) further indicates that in certain theoretical limits Δt_s can approach the WS time delay Δt_{WS} . In particular, for short-range potentials $V(x)$, Δt_s is approximately given by the first term (i.e., $j = 1$) of the sum in Eq. (10) if the electron wave packet propagates over the full range of the potential during $[t_i, t_i + \delta t]$, while $E_s(t) \simeq E_s(t_i)$. This condition should be fulfilled in the following theoretical limits: (a) the effective range of $V(x)$ goes to zero, (b) the momentum of the electron goes to infinity, or (c) the oscillation period of the streaking field goes to infinity. To test our expectations, we performed simulations for the 1D potential

$$V(x) = V_{C-WS}(x) = -\frac{Z}{\sqrt{x^2 + a}} \frac{1}{1 + e^{(|x| - x_p)/b}}, \quad (11)$$

which is a product of Coulomb and Woods-Saxon potentials, where x_p determines the effective range of the potential.

We have chosen $b = 1$ and $x_p \geq 10$ such that $V_{C-WS} \simeq V_C$ for $|x| < x_p$, while V_{C-WS} approaches zero quickly for $|x| > x_p$. To obtain the WS time delays, we used the back-propagation method introduced in Refs. [23,24]. In Fig. 4 we compare the results of the numerical simulations for Δt_s (solid lines with circles and diamonds) as a function of (a) the potential range x_p , (b) the frequency of the ionizing XUV pulse, and (c) the wavelength of the streaking pulse with the WS time delay Δt_{WS} [dashed lines with squares for (a) and (b) and solid circles for (c)]. All other parameters of the fields are kept the same in the simulations. As expected, Δt_s approaches Δt_{WS} in each of the three theoretical limits listed above.

D. Interpretation of other features in the numerical results

We note that more subtle features in our TDSE results, such as the oscillations in Fig. 1(a) and the change from a decrease to an increase in Δt_s as a function of x_p in Fig. 4(a) can also be well understood from the classical formulas. The oscillations in Fig. 1(a) are caused by the Gaussian potential, which has a very short effective range. The streaking delay contribution due to the Gaussian potential can be therefore written as

$$\Delta t_s^G(x_0) \simeq \frac{E_s(t_G)}{E_s(t_i)} \Delta t_{WS}^G, \quad (12)$$

where t_i and t_G are the instant of ionization and the time instant at which the electron reaches the Gaussian potential, respectively. Thus, the streaking time delay induced by the coupling of the streaking field and the Gaussian potential should have an oscillation period proportional to that of the streaking field, which can be easily confirmed from the results in Fig. 1(a) by noting that $t_G \simeq z_0/k_0$.

The nonmonotonic behavior of the streaking time delay in Fig. 4(a) can be explained by Eq. (8). Assuming that the electron is ionized at the peak of the streaking field, the absolute value of the time delay is expected to increase over the first quarter of the streaking field cycle. However, then the field changes sign and the absolute value should start decreasing. The turning point at $x_p = 50$ agrees well with the classical estimate for the distance the electron travels within the first quarter cycle after its release, namely $x_{wp} = k_0 T_s / 4 = 54$ at the present parameters.

E. Application to 3D cases

In Fig. 5 we show that the predictions of the classical approximations, Eqs. (7) and (8), are in good agreement with the results for the time delay Δt_s obtained in other recently reported numerical streaking simulations for the hydrogen atom and the helium ion. In these studies [4,13,17] full 3D quantum simulations have been performed. The agreement clearly supports our conclusions based on 1D classical analysis.

Before concluding, we discuss the implication of our analysis on the experimental observations of a relative time delay between the photoemission from the $2s$ and $2p$ shells in the neon atom [3]. Based on our classical approximation we estimate a time delay Δt_s of about -5.2 as for the emission from the $2p$ shell and of about -9.7 as for the $2s$ electron. These numbers are obtained using single-active electron potentials and the field parameters given in Ref. [3].

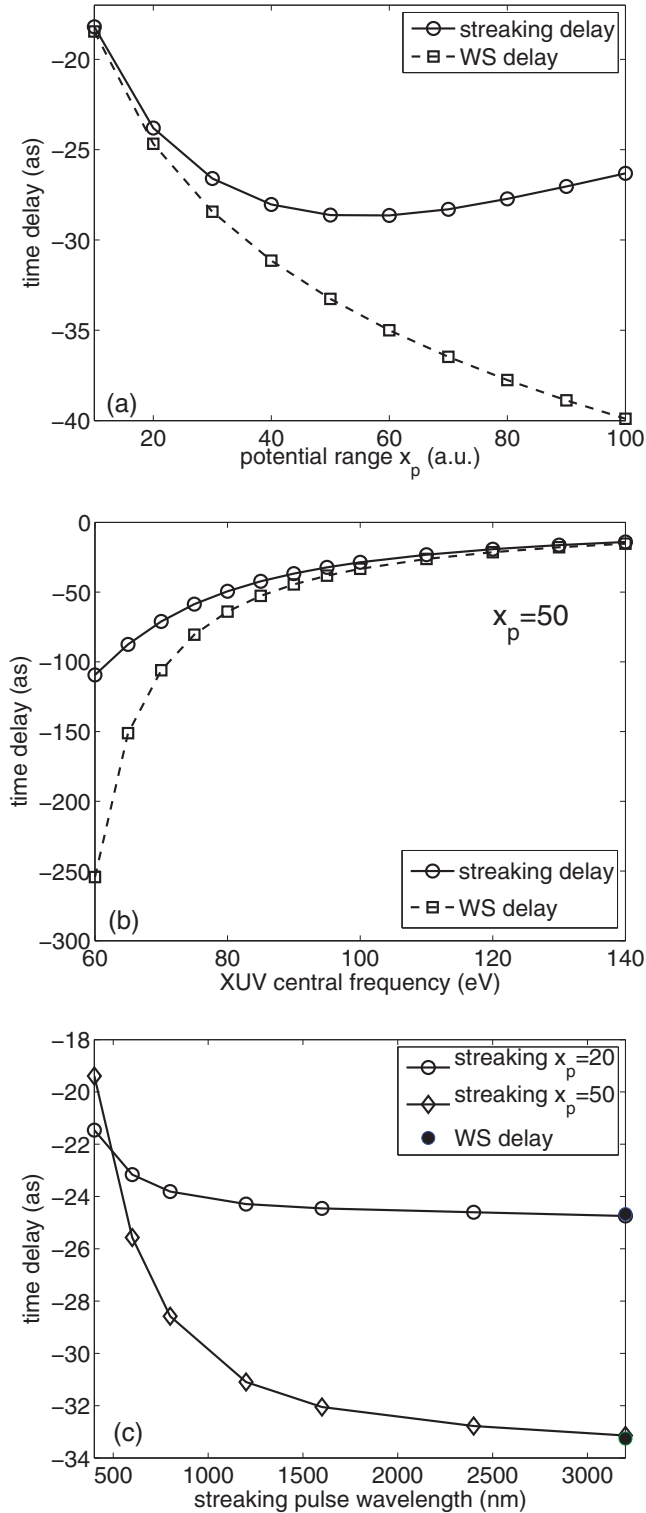


FIG. 4. (Color online) Results of numerical simulations for the streaking time delays Δt_s (solid line with circles and diamonds) as a function of (a) the range x_p of a short-range potential, (b) the frequency of the ionizing XUV field, and (c) the wavelength of the streaking pulse are compared with those for the WS time delay [dashed lines with squares in (a) and (b) and solid circles in (c)]. Laser parameters are: $I_{\text{XUV}} = 1 \times 10^{15}$ W/cm², $T_{\text{XUV}} = 600$ as, $\omega_{\text{XUV}} = 100$ eV [(a),(c)], $\phi_{\text{XUV}} = -\pi/2$, $I_s = 1 \times 10^{12}$ W/cm², $N_s = 3$ cycle [(a),(b)], $T_s = 32.02$ fs [(c)], $\lambda_s = 800$ nm [(a),(b)], and $\phi_s = -\pi/2$.

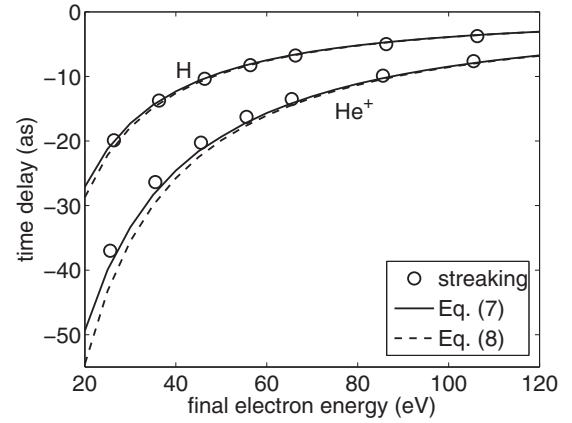


FIG. 5. Comparison of time delays from 3D quantum streaking simulations (open circles, extracted from Ref. [13]) with the results of the present classical approximations, Eq. (7) (solid lines) and Eq. (8) (dashed lines). For both potentials the initial states are chosen to be the $1s$ state. The parameter α varied between 1.003 and 1.067.

Thus, we estimate a relative time delay of about 4.5 as, which cannot fully account for the experimentally observed time delay of 21 as. Based on our analysis we conclude that many-body effects (e.g., [9,17,28]) or the influence of other factors, as discussed in Ref. [3], which would be considered in the potential V , may contribute to Δt_s via a coupling with the streaking field as well.

III. CONCLUSIONS

In summary, our results show that the time delay in numerical streaking simulations arises from the electron dynamics in the coupled potential of the Coulomb and the streaking fields and therefore strongly depends on the parameters, in particular the duration, of the streaking field. The delay accounts for the finite range of the potentials in space over which the electron propagates after its emission until the streaking pulse ceases. It can be represented as an integral or sum over field-free time delays weighted by the instantaneous streaking field strength relative to the field strength at the time of ionization.

ACKNOWLEDGMENTS

J.S. and A.B. acknowledge support by a grant from the U.S. Department of Energy, Division of Chemical Sciences, Atomic, Molecular and Optical Sciences Program. H.N. was supported via a grant from the U.S. National Science Foundation (Award No. PHY-0854918). A.J.-B. was supported by grants from the U.S. National Science Foundation (Awards No. PHY-1125844 and No. PHY-1068706). This work utilized the Janus supercomputer, which is supported by the National Science Foundation (Award No. CNS-0821794) and the University of Colorado Boulder. The Janus supercomputer is a joint effort of the University of Colorado Boulder, the University of Colorado Denver and the National Center for Atmospheric Research. Janus is operated by the University of Colorado Boulder.

- [1] F. Krausz and M. Ivanov, *Rev. Mod. Phys.* **81**, 163 (2009).
- [2] A. L. Cavalieri, N. Müller, T. Uphues, V. S. Yakovlev, A. Baltuška, B. Horvath, B. Schmidt, L. Blümel, R. Holzwarth, S. Hendel, M. Drescher, U. Kleineberg, P. M. Echenique, R. Kienberger, F. Krausz, and U. Heinzmann, *Nature (London)* **449**, 1029 (2007).
- [3] M. Schultze *et al.*, *Science* **328**, 1658 (2010).
- [4] K. Klünder, J. M. Dahlström, M. Gisselbrecht, T. Fordell, M. Swoboda, D. Guénot, P. Johnsson, J. Caillat, J. Mauritsson, A. Maquet, R. Taïeb, and A. L'Huillier, *Phys. Rev. Lett.* **106**, 143002 (2011).
- [5] J. Itatani, F. Quéré, G. L. Yudin, M. Y. Ivanov, F. Krausz, and P. B. Corkum, *Phys. Rev. Lett.* **88**, 173903 (2002).
- [6] We use Hartree atomic units, $e = m = \hbar = 1$, throughout this paper.
- [7] E. P. Wigner, *Phys. Rev.* **98**, 145 (1955).
- [8] F. T. Smith, *Phys. Rev.* **118**, 349 (1960).
- [9] A. S. Kheifets and I. A. Ivanov, *Phys. Rev. Lett.* **105**, 233002 (2010).
- [10] I. A. Ivanov, *Phys. Rev. A* **83**, 023421 (2011).
- [11] I. A. Ivanov, *Phys. Rev. A* **86**, 023419 (2012).
- [12] C.-H. Zhang and U. Thumm, *Phys. Rev. A* **84**, 033401 (2011).
- [13] S. Nagele, R. Pazourek, J. Feist, K. Doblhoff-Dier, C. Lemell, K. Tökési, and J. Burgdörfer, *J. Phys. B* **44**, 081001 (2011).
- [14] M. Ivanov and O. Smirnova, *Phys. Rev. Lett.* **107**, 213605 (2011).
- [15] J. M. Dahlström, A. L'Huillier, and A. Maquet, *J. Phys. B* **45**, 183001 (2012).
- [16] J. M. Dahlström, D. Guénot, K. Klünder, M. Gisselbrecht, J. Mauritsson, A. L'Huillier, A. Maquet, and R. Taïeb, *Chem. Phys.* **414**, 53 (2013).
- [17] S. Nagele, R. Pazourek, J. Feist, and J. Burgdörfer, *Phys. Rev. A* **85**, 033401 (2012).
- [18] R. Pazourek, J. Feist, S. Nagele, and J. Burgdörfer, *Phys. Rev. Lett.* **108**, 163001 (2012).
- [19] C.-H. Zhang and U. Thumm, *Phys. Rev. A* **82**, 043405 (2010).
- [20] J. C. Baggesen and L. B. Madsen, *Phys. Rev. Lett.* **104**, 043602 (2010).
- [21] M. D. Spiewanowski and L. B. Madsen, *Phys. Rev. A* **86**, 045401 (2012).
- [22] R. Pazourek, S. Nagele, and J. Burgdörfer, *Faraday Discuss.* **163**, 353 (2013).
- [23] J. Su, H. Ni, A. Becker, and A. Jaroń-Becker, *Phys. Rev. A* **87**, 033420 (2013).
- [24] J. Su, H. Ni, A. Becker, and A. Jaroń-Becker, *J. Mod. Opt.* (2013), doi: [10.1080/09500340.2013.778342](https://doi.org/10.1080/09500340.2013.778342).
- [25] The instant of ionization here and in the remainder of the paper stands for the time instant of the transition of the electron into the continuum.
- [26] P. B. Corkum, *Phys. Rev. Lett.* **71**, 1994 (1993).
- [27] A similar expression has been used in the classical-trajectory Monte Carlo simulations for streaking experiments in Ref. [13].
- [28] L. R. Moore, M. A. Lysaght, J. S. Parker, H. W. van der Hart, and K. T. Taylor, *Phys. Rev. A* **84**, 061404 (2011).